

Symbolic Equation Solving via Reinforcement Learning

Lennart Dabelow

L.DABELOW@QMUL.AC.UK

RIKEN Center for Emergent Matter Science (CEMS), Wako, Saitama 351-0198, Japan

School of Mathematical Sciences, Queen Mary University of London, London E1 4NS, UK

Masahito Ueda

UEDA@CAT.PHYS.S.U-TOKYO.AC.JP

Department of Physics and Institute for Physics of Intelligence, Graduate School of Science,

The University of Tokyo, Bunkyo-ku, Tokyo 113-0033, Japan

RIKEN Center for Emergent Matter Science (CEMS), Wako, Saitama 351-0198, Japan

Abstract

Machine-learning methods are gradually being adopted in a wide variety of social, economic, and scientific contexts, yet they are notorious for struggling with exact mathematics. A typical example is computer algebra, which includes tasks like simplifying mathematical terms, calculating formal derivatives, or finding exact solutions of algebraic equations. Traditional software packages for these purposes are commonly based on a huge database of rules for how a specific operation (e.g., differentiation) transforms a certain term (e.g., sine function) into another one (e.g., cosine function). These rules have usually needed to be discovered and subsequently programmed by humans. Efforts to automate this process by machine-learning approaches are faced with challenges like the singular nature of solutions to mathematical problems, when approximations are unacceptable, as well as hallucination effects leading to flawed reasoning. We propose a novel deep-learning interface involving a reinforcement-learning agent that operates a symbolic stack calculator to explore mathematical relations. By construction, this system is capable of exact transformations and immune to hallucination. Using the paradigmatic example of solving linear equations in symbolic form, we demonstrate how our reinforcement-learning agent autonomously discovers elementary transformation rules and step-by-step solutions.

Keywords: reinforcement learning, symbolic mathematics, computer algebra, deep Q learning, adversarial learning

1 Introduction

Deep learning and artificial intelligence have become ubiquitous tools in industry and academia, demonstrating automatic data-processing and control capabilities with unprecedented speed and accuracy. In general, deep-learning schemes are known to excel in statistical and approximation settings, where many similar problems and/or solutions exist. Remarkable success stories include robots with robust motoric skills (Lee et al., 2020; Andrychowicz et al., 2020), the development of super-human strategic game engines (Mnih et al., 2015; Silver et al., 2017, 2018; Perolat et al., 2022; Wurman et al., 2022; Bakhtin et al., 2022), and most recently the ability of large language models to produce human-like texts on seemingly arbitrary topics (Brown et al., 2020; Chowdhery et al., 2022; Thoppilan et al., 2022; OpenAI, 2023; Touvron et al., 2023; BigScience Workshop: T. Le Scao *et al.*, 2023).

Nevertheless, these methods continue to struggle with the rigor and exactness required for mathematical reasoning and deduction (Choi, 2021; Ornes, 2020; Bubeck et al., 2023;

Wolfram, 2023b). In this domain, problems often have only one or a handful of solutions, and to find them, a certain sequence of steps or transformations needs to be carried out precisely and in the right order. Consider, for instance, an equation like $3x + 2c = x + 4$ with the unknown x and a symbolic parameter c . It has one and only one exact solution, $x = 2 - c$ (up to symmetries), but no “approximately acceptable” answers, and a number of equivalence transformations need to be performed in sequence to arrive at that solution.

Another caveat of several traditional AI methods and large language models in particular is their proneness to hallucination (Maynez et al., 2020; Ji et al., 2023), meaning that they can come up with false claims and sell them apparently convincingly. These flaws are inherent to the probabilistic, creativity encouraging architecture of these models. In fact, one could argue that the models were not designed to carry out rigorous mathematics, but they are still being employed in this way in practice (Wei et al., 2022; Drori et al., 2022; Lewkowycz et al., 2022; Bubeck et al., 2023; Wolfram, 2023a).

In this work, we put forward a reinforcement-learning (RL) platform that allows a neural network to discover autonomously how to solve mathematical equations. As introduced in detail in Section 2.2, the idea is that the so-called RL agent explores an environment and tries to maximize the rewards it receives for certain expedient actions. In our case, the environment involves a stack calculator (see Section 2.4) that can represent and manipulate mathematical expressions in symbolic form. The RL agent works on the calculator to explore transformations, is rewarded for finding a solution to a given equation, and thereby learns solution strategies.

The main virtues of our RL approach are: (i) The agent learns independently, i.e., no solutions or solution strategies need to be known or provided a priori. (ii) Whenever the agent comes up with a solution, it is guaranteed to be correct by construction, hence the approach is immune to hallucination effects. (iii) The solutions are presented in a step-by-step fashion, meaning that the reasoning is transparent and easily comprehensible for humans.

In Section 2, we introduce the method and its background in detail. Thereafter, we analyze our approach on a diverse set of linear equations involving real-valued, complex-valued, and symbolic coefficients in Section 3 and discuss the results and their relation to previous work in Section 4.

2 Reinforcement learning on a symbolic stack calculator

2.1 Outline

Our idea is to replace conventional software packages to deal with exact mathematics, namely so-called computer algebra systems (CAS) such as Mathematica, Maple, Matlab, or SymPy, by a new reinforcement-learning-based symbolic stack calculator. CAS can analyze and manipulate mathematical terms symbolically, i.e., in an analytically exact manner. With their functionality covering almost all areas of mathematics, they have become an indispensable tool in scientific research and education. Common use cases include term simplification, calculus, and solving algebraic equations.

The core of such CAS is typically a database of rules that encode how a specific term pattern A is transformed into another pattern B if operation T is applied,

$$\text{operation } T : \text{ term } A \rightarrow \text{ term } B. \quad (1)$$

To implement a differentiation module, for example, one elementary rule could be “ $\partial/\partial x : \sin x \rightarrow \cos x$.” A powerful CAS builds on a vast number of such elementary transformation rules. All of these rules first had to be found by humans, a process that has lasted for millennia in the form of mathematical research. In a second step, humans must implement the discovered rules as computer programs. Evidently, this procedure could benefit greatly from techniques that enable computers to start from a certain set of definitions and established rules and combine them to discover and implement new transformation rules on their own. Moreover, finding viable approaches to do so will eventually help to make machine-learning models more adept at mathematics and problems requiring exact solutions in general.

In the following, we develop a deep reinforcement-learning scheme that can autonomously find elementary transformation rules for the symbolic solution of algebraic equations, a key component of CAS functionality. To illustrate this task, two basic rules of such a CAS module could be

$$\text{solve for } x: x + a_0 = b_0 \ (a_0, b_0 \in \mathbb{C}) \rightarrow x = b_0 - a_0 \quad (2)$$

and

$$\text{solve for } x: a_1 x = b_0 \ (a_1 \in \mathbb{C} \setminus \{0\}, b_0 \in \mathbb{C}) \rightarrow x = b_0/a_1. \quad (3)$$

To solve the more complicated problem $a_1 x + a_0 = b_0$, we can define a third rule that decomposes the problem: To solve $f(x) + a_0 = b_0$ for x , first solve for $f(x)$ (using rule (2)), then solve for x (using rule (3) in this case). This way, complex equations can be disentangled and eventually solved.

2.2 Deep Reinforcement Learning

We set up a reinforcement learning (RL) framework that facilitates the automatic discovery and implementation of transformation rules. As usual, it involves an *agent*, whose role is to suggest the transformation rules, and an *environment*, which consists of the equation to be solved and some auxiliary information. We briefly recall a few key concepts here to introduce notation and refer to the reviews (Arulkumaran et al., 2017; Sutton and Barto, 2018; Marquardt, 2020) for a more in-depth exposition as well as to Appendix A for technical details of our implementation.

The RL agent learns through a feedback loop as illustrated in Fig. 1: In every time step t , it makes an observation $s_t = v(q_t)$ of the state q_t of the environment and subsequently chooses an action a_t according to a conditional probability distribution (“policy”) $\pi(a_t | s_t)$. The environment responds to this action by changing its state into a new one, q_{t+1} . Furthermore, it issues a reward r_t , which is positive if the action was beneficial for the task, negative if it was adverse, or zero if the implications are unclear. On the basis of these rewards, the agent may update its policy in an attempt to maximize the expected future return $V_\pi(s) := \mathbb{E}_\pi[\sum_{t=0}^{\infty} \gamma^t r_t | s_0 = s]$ for all states s , where $\gamma \in [0, 1)$ is a discount factor to ensure convergence.

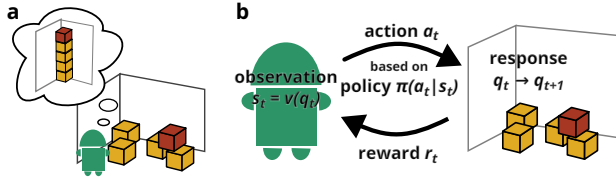


Figure 1: Schematic illustration of the reinforcement-learning approach. (a) An agent interacts with its environment and is supposed to solve a specific task. (b) Learning proceeds via a feedback loop: The agent makes an observation $s_t = v(q_t)$ of the state q_t of the environment and decides on its next action a_t according to the policy $\pi(a_t | s_t)$ (conditional probability distribution). The environment responds to the action by changing its state and issuing a reward r_t that reflects how close the new state is to the desired goal. The agent updates its policy with the aim of maximizing the accumulated rewards.

We adopt the Q -learning approach based on the quality function

$$Q(s, a) := \mathbb{E} \left[\sum_{t=0}^{\infty} \gamma^t r_t \mid s_0 = s, a_0 = a \right]. \quad (4)$$

It is obtained from V_π by splitting off and conditioning on the first action a , and subsequently following a greedy policy with respect to Q itself, meaning that we always choose the action that maximizes Q in the present state, $a_t = \arg \max_a Q(s_t, a)$, for $t \geq 1$. The Q function of the optimal policy, which yields the largest discounted return, satisfies the Bellman equation (Arulkumaran et al., 2017; Sutton and Barto, 2018; Marquardt, 2020),

$$Q(s_t, a_t) = \mathbb{E} \left[r_t + \gamma \max_a Q(s_{t+1}, a) \right]. \quad (5)$$

Implementing double deep Q -learning (Hasselt et al., 2016), we train a neural network f_θ with parameters θ to represent Q . The network receives the observed state s and maps it onto a vector whose components are the values of Q for each action a , i.e., $Q(s, a) = [f_\theta(s)]_a$. The parameters θ are updated with the goal of solving the Bellman equation (5), see Appendix A.3 for details.

2.3 Equation Classes

As explained above, we focus on the task of finding exact solutions for linear equations. More specifically, we consider two main types of equation classes. The first one consists of linear equations of the general form

$$a_0 + a_1 x = a_2 + a_3 x, \quad (6)$$

where x is the variable to solve for and the coefficients a_i are numbers taken from \mathbb{Z} , \mathbb{Q} , \mathbb{R} , or \mathbb{C} ; the specific choices constitute several subclasses.

The second type involves one additional symbolic parameter c and consists of equations of the form

$$a_0 + b_0 c + (a_1 + b_1 c) x = a_2 + b_2 c + (a_3 + b_3 c) x, \quad (7)$$

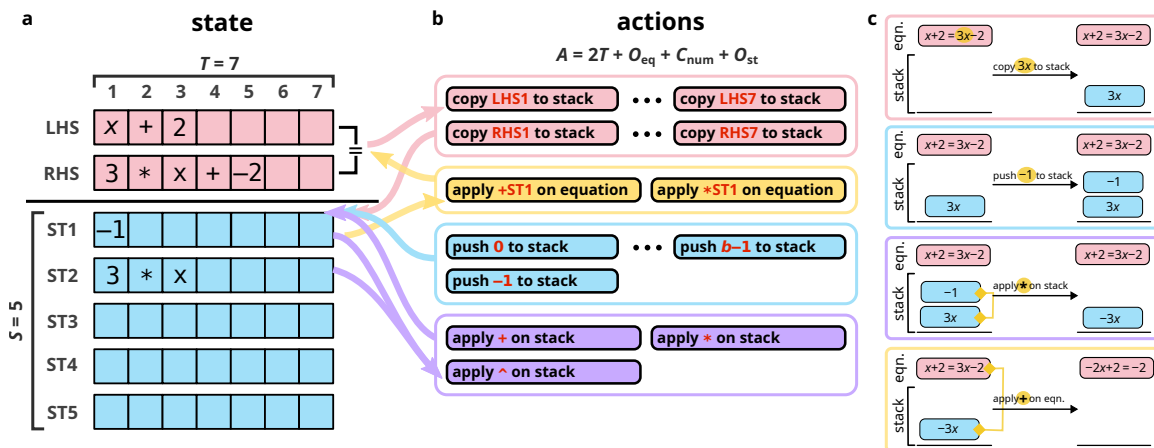


Figure 2: Main components of the reinforcement-learning framework for symbolic equation solving. (a) The state comprises the left- and right-hand sides of the equation as well as a stack of up to S additional terms. Every term consists of (up to) T elementary units (i.e., operators, variables, numbers, parentheses). (b) The agent can choose from four classes of actions: copy (sub)terms from the equation to the stack ($2T$ actions); perform an equivalence transformation of the equation (O_{eq}); push a predefined numerical constant to the stack (C_{num}); or apply a mathematical operation on the stack (O_{st}). (c) Examples of how the state changes under each of the four classes of actions.

where $a_i, b_i \in \mathbb{Z}, \mathbb{Q}, \mathbb{R},$ or \mathbb{C} as before. Importantly, mastering this problem enables the machine to solve *systems* of symbolic equations as well by solving one equation for the first variable (e.g., x), substituting the solution into the second equation, and solving for the second variable (c), and so on if there are more than two variables.

During training, we generate an equation of the form (6) or (7) whenever a new task is assigned by sampling the coefficients a_i, b_i randomly from an appropriate distribution (see Appendix A.1 for details). For testing, we use fixed sets of example equations generated in the same way and provided as supplementary material for reference. We also explore an adversarial approach where training problems are generated by a second RL agent. As explained in more detail below, the goal of this generator agent is to find as simple a problem as possible such that the solver agent fails.

2.4 Environment and Actions: The Stack Calculator

The key ingredients of our specific RL framework and the symbolic stack calculator are illustrated in Fig. 2. The first component of our RL environment is the equation, initially given in the form (6) or (7), for example. It consists of two mathematical expressions (terms), namely the left-hand side (LHS) and the right-hand side (RHS), cf. Fig. 2a.

The agent is to carry out a sequence of equivalence transformations that either cast the equation into the form

$$x = (\text{something independent of } x) \quad (8)$$

or eliminate the variable x from it if the original equation was ill-defined. Once this is achieved, we consider the problem to be solved. If the agent fails to reach such a state within t_{\max} elementary steps, we consider the attempt to be unsuccessful.

To suggest the right sequence of transformations, the agent must be able to perform all the mathematical operations occurring in the equation or, more precisely, the corresponding inverse operations. We implement this ability by giving the agent access to a stack calculator that can manipulate terms in symbolic form. This is the second component of our RL environment (cf. Fig. 2a). It consists of a stack of up to S terms. Whenever a new term is added to the stack, it is inserted in the top position and all entries move down accordingly. We can compose arbitrary mathematical operations by taking a fixed number of terms from the top of the stack, feeding them into a predefined function, and pushing the result back onto the stack. For example, the operation “+” removes the first two terms from the stack, adds them together, and deposits the sum on the stack again. Provided that the stack calculator supports all relevant operations, this enables the agent to prepare and eventually execute all necessary equivalence transformations to solve the equation. This universality is our first main motivation to carry out RL on a stack calculator.

Specifically, the agent can choose from four different types of actions for this purpose, cf. Fig. 2b. The first type allows it to copy a (sub)term from the left- or right-hand side of the equation to the stack (cf. Fig. 2c for an example). To this end, every term is decomposed into up to T elementary units, which are operators (+, *, ^), variables (x , c), numbers (2 , $-\frac{1}{3}$, $\sqrt{2}$), or parentheses. The agent can select any of those elementary units for copying. For units consisting of operators or parentheses, the entire associated subterm will be cloned. This gives a total of $2T$ “copy” actions.

The second action type involves pushing one of C_{num} predefined numerical constants to the stack. These typically include the numbers 0 and 1 (basis of the binary number system), -1 (frequently needed for inverse operations), and i (imaginary unit) in the case of complex-valued coefficients a_i , b_i in Eqs. (6)–(7). Pushing several 0s and/or 1s sequentially is interpreted as providing the binary digits of an integer.

The third action type applies one of O_{st} specific mathematical operations on the stack as outlined above. In our case, $O_{\text{st}} = 3$ with addition “+”, multiplication “*” and exponentiation “^”.

Finally, the fourth type facilitates the actual equivalence transformation by performing one of O_{eq} specific mathematical operations on both sides of the equation, possibly involving additional arguments from the stack. In our case, in particular, we have $O_{\text{eq}} = 2$ with addition “+” and multiplication “*”, both of which take the top entry from the stack as the second operand.

By skillful assembly of these actions in the right order, the agent can then transform any equation of the initial forms (6)–(7) into the goal state (8). The four steps taken in Fig. 2c provide one example of a sequence that serves to eliminate the variable x from the right-hand side. A full, machine-solved example can be found in Fig. 3d.

To avoid any human bias about what the optimal strategy is, we only issue a positive reward r_{slv} when the agent reaches the goal and achieves a state of the form (8) or eliminates x for ill-defined problems. Furthermore, we deduct from this final reward r_{slv} a penalty p_{st} for every term that is left on the stack and a penalty p_{as} for any assumptions that are necessary during the transformation (e.g., $x \neq 0$ if the equation is divided by x), see also

Appendix A.6. The idea of these penalties is to encourage concise solution strategies that avoid redundant and unnecessary steps.

This general framework can be extended to other types of algebraic equations by suitably adjusting the available operations for equation and stack manipulations. This expandability is our second main motivation for following the stack-calculator approach.

Furthermore, our philosophy is for the agent to focus on the equation-solving logic: The agent should understand the structure of the equation and devise the correct inverse transformation. However, it should not be bothered with the algebraic simplification of mathematical expressions (e.g., $3 \times 2 \rightarrow 6$ or $-2x + 5x \rightarrow 3x$). Such simplifications are instead performed automatically in the environment using SymPy (Meurer et al., 2017), cf. Appendix A.7. In a future, more autonomous and machine-learned CAS, we envision that this process could be handled by a different RL agent or module that is specialized in term simplification. Likewise, other SymPy features could be replaced or added using machine learning.

3 Analysis

We will demonstrate our RL approach to equation solving on several types of problems. In Section 3.1, we focus on equations with numerical coefficients (type (6)) from the integers, reals, or complex numbers. In Sections 3.2 and 3.3, we will increase the complexity by admitting additional symbolic coefficients (type (7)). We will use randomly generated training problems in Sections 3.1 and 3.2, whereas we will explore the benefits and limitations of adopting an adversarial problem generator in Section 3.3. We will compare all approaches with each other in their common domains.

3.1 Purely Numerical Coefficients

We concentrate on equations of type (6) with real-valued coefficients first. In Fig. 3a, we monitor the test success rate (i.e., the fraction of successfully solved problems from a fixed set of test equations) as a function of the training time τ (i.e., the number of parameter updates). Training initially uses only integer coefficients ($a_i \in \mathbb{Z}$ in Eq. (6)), corresponding to the solid lines in the figure. After an initial exploration period of around 5×10^6 training epochs with only sporadic success, the performance drastically improves, reaching success rates of almost 100% on the test set with integer coefficients (top-left panel of Fig. 3a). At the same time, we observe that only about 50% of equations with rational coefficients are solved successfully (top-right panel of Fig. 3a). Hence we start a second training scheme using equations with coefficients $a_i \in \mathbb{Q}$ from this point (dashed lines in Fig. 3). This way, we eventually achieve success rates $\geq 99.8\%$ on both the integer- and rational-coefficient test sets. We point out that there is no conceptual generalization in admitting irrational coefficients because the state encoding presented to the agent only provides floating-point representations of numerical constants (cf. Appendix A.2), i.e., the agent will deal with rational and general real-valued coefficients in the same way.

In the lower panels of Fig. 3a, we also show the average number of steps required for solved tasks (restricted to machines with success rates $\geq 2\%$), which quantifies the computational complexity of the learned solution strategies. Initially, solutions are found somewhat accidentally and therefore require a large number of steps. Once the agent has

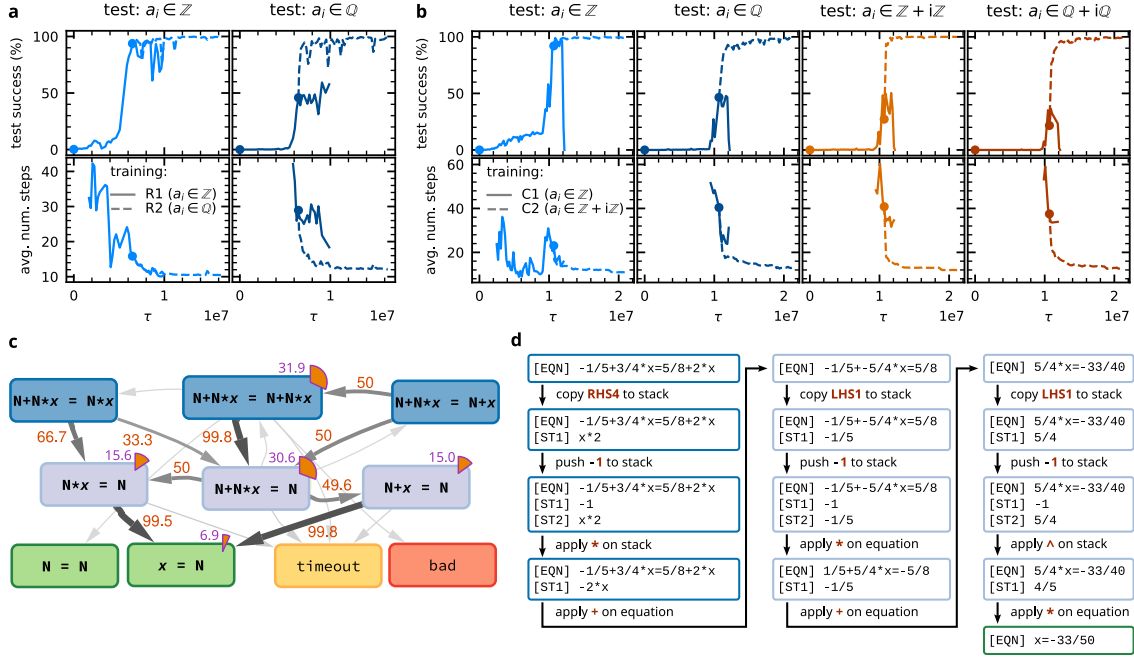


Figure 3: Test success and solution strategies for equations of type (6) with (a) real-valued coefficients or (b–d) complex-valued coefficients. (a, b) Test success and average number of elementary steps to success vs. training time τ for various test data sets (see column heading) and maximum number of steps $t_{\max} = 100$. Average number of steps (bottom row) only shown if test success is $\geq 2\%$. (a) Solid (R1): training with integer a_i ; dashed (R2): training with rational a_i . (b) Solid (C1): training with real-integer a_i ; dashed (C2): training with complex-integer a_i . (c) Summary graph for the solution strategy of (C2) after $\tau = 1.955 \times 10^7$ training epochs, analyzed for the complex-rational test data set. States are collected into superstates according to the form of the equation, disregarding left-right symmetry and the stack. Disk sectors and numbers (in purple) indicate the relative number of elementary steps spent in the respective superstates (in %, only shown if $\geq 1\%$). Transitions between superstates are indicated by arrows, with their relative frequencies compared to all transitions from a fixed state given by the numbers in red (in %, only shown if $\geq 1\%$). Special states: *timeout*: SymPy processing of the selected action exceeds 10s; *bad*: state cannot be represented as a neural-network tensor (e.g., term size exceeds T , numerical overflow). (d) Example sequence of elementary transformations suggested by the network from (c) to solve $-\frac{1}{5} + \frac{3}{4}x = \frac{5}{8} + 2x$.

managed to achieve some consistency, the required number of steps goes down and gradually decreases further as the strategy is fine-tuned. Except for special cases (e.g., when some of the coefficients in Eqs. (6) or (7) vanish), the number of steps needed by a specific agent will be very similar across problems from a given class.

For complex-valued coefficients a_i in Eq. (6), the results in Fig. 3b show very similar characteristics. Starting with training on real-integer coefficients (solid lines), the agent makes gradual progress until the success rate abruptly improves at around $\tau = 10^7$ (top-left panel of Fig. 3b). At this point, the agent also starts managing to solve some of the problems with more general coefficient types (second to fourth columns in Fig. 3b). However, continued training with real-integer coefficients soon becomes unstable, leading to diverging parameter updates, a common side effect of deep Q -learning (Sutton and Barto, 2018; van Hasselt et al., 2018; Wang and Ueda, 2022). Switching to complex-integer coefficients instead (dashed lines) yields further improvement of the test success, with eventual success rates $\geq 98.9\%$ across all different test sets. We particularly highlight that the agent generalizes from training on complex-integer coefficients to near-perfect success rates on complex-rational coefficients (cf. top-right panel of Fig. 3b).

In Fig. 3c, we illustrate the solution strategy of one of the best agents on the equations with complex-rational coefficients. For clarity, we group states according to their equation structure. The graph visualizes the transitions between the resulting superstates, highlighting their relative frequencies among all transitions from a given superstate. Typically, an initial sequence of transformation steps serves to eliminate the variable from one side of the equation (top to middle layer in Fig. 3c), which most commonly results in equations of the form $a_0 + a_1x = b_0$ (middle node of the middle layer). From here, the agent proceeds in two different ways without significant preference: Either it subtracts a_0 , leading to the $N*x=N$ pattern (left node of the middle layer) or it divides by a_1 and ends up in the $N+x=N$ superstate (right node). This is one incidence of a more general observation that the strategies discovered by the agent tend to be more fine-grained than the recipes typically taught to humans. The final transformation then consists of the pertinent division or subtraction, leading to the solution state $x=N$. A concrete example with the detailed states and elementary transformations as suggested by this agent is given in Fig. 3d.

3.2 Mixed Symbolic and Numerical Coefficients

Next we turn to the second type of equations, cf. Eq. (7), which feature a second symbolic variable c besides the unknown x . Note that this problem is considerably more complex than type (6) because of much greater term variety and sizes, which additionally lead to a larger action space. Test results for various training schemes and test types are shown in Fig. 4, monitoring the success rate and the average number of steps required for successfully solved equations.

As before, we follow a training strategy that gradually increases the problem complexity. We begin with a simplified version where either $a_0 = b_0 = a_3 = b_3 = 0$ or $a_1 = b_1 = a_2 = b_2 = 0$ in Eq. (7) (label S1, solid lines). Once the agent has learned to deal with these structurally simpler equations, we switch to the full form, focusing on $a_i, b_i \in \mathbb{Z}$ first (S2 and S3, dotted and dash-dotted lines). The S2 and S3 training schemes differ in the frequency of symbolic coefficients and some of the hyperparameters (see Appendix C). During the S2 stage, the agent first learns to solve equations with purely numerical coefficients, similar to type (6), after around $\tau \approx 10^7$ epochs (cf. the first and second columns of Fig. 4), but initially struggles with equations involving the parameter c (third and fourth columns). As it improves its solution capabilities for the latter type of symbolic problems, it temporarily

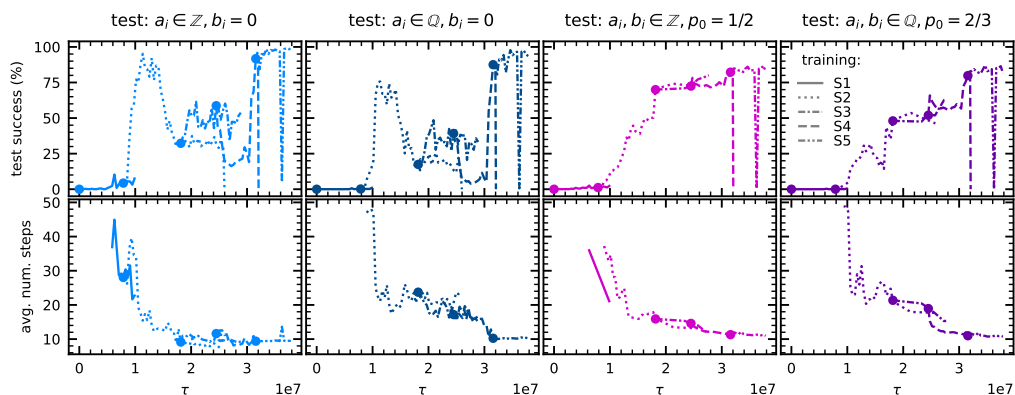


Figure 4: Test success and average number of steps for equations of type (7) with mixed numerical (real-valued) and symbolic coefficients. Test types: see column headings; maximum number of steps: $t_{\max} = 100$. Solid (S1): training with $a_i, b_i \in \mathbb{Z}$ and $a_0 = b_0 = a_3 = b_3 = 0$ or $a = 1 = b_1 = a_2 = b_2 = 0, p_0 = 0$, learning rate $\eta = 0.05$; dotted (S2): training with $a_i, b_i \in \mathbb{Z}, p_0 = 1/2, \eta = 0.05$; dash-dotted (S3): training with $a_i, b_i \in \mathbb{Z}, p_0 = 2/3, \eta = 0.01$; dashed (S4): training with $a_i, b_i \in \mathbb{Q}, p_0 = 2/3, \eta = 0.05$; dash-dot-dotted (S5): training with $a_i, b_i \in \mathbb{Q}, p_0 = 2/3, \eta = 0.01$. Average number of steps for successful transformations (bottom row) only shown if test success is $\geq 2\%$.

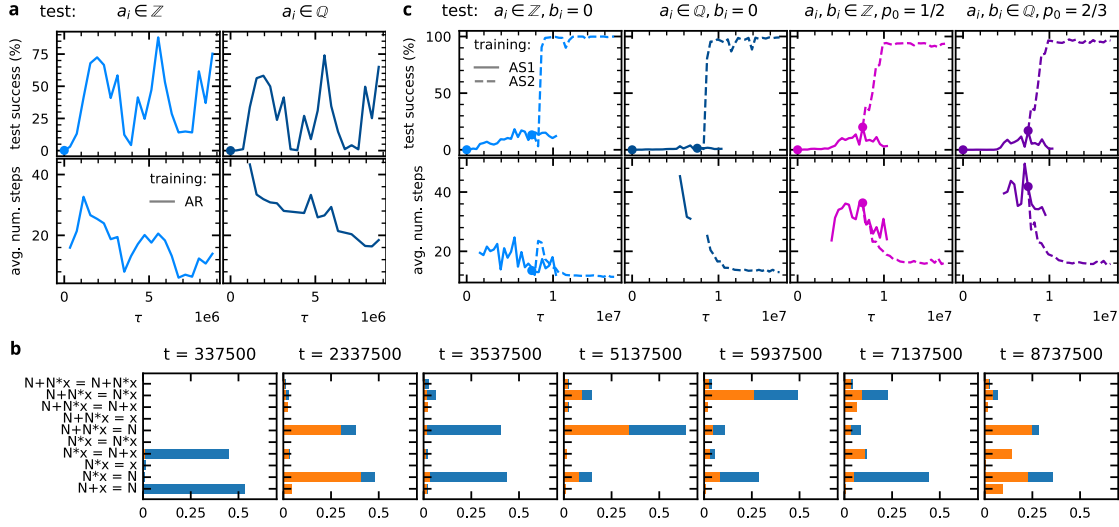


Figure 5: Characteristics of the adversarial reinforcement-learning approach. (a) Test success and average number of steps for equations with purely numerical coefficients (test types: see column headings). Generator initialization: $x = a \in \mathbb{Q}$ (see also Appendix A.1). (b) Histograms of the equation patterns produced by the generator (blue) and the fraction of successfully recovered solutions by the solver (orange). (c) Test success and average number of steps for equations with mixed symbolic and numerical coefficients (test types: see column headings). Solid (AS1): adversarial training, generator initialization $x = (a_1 + b_1c)/(a_2 + b_2c)$ with $a_i, b_i \in \mathbb{Q}$, $p_0 = 1/2$; dashed (AS2): fixed-distribution training with equation type (7), $a_i, b_i \in \mathbb{Q}$, $p_0 = 2/3$. Learning rates and greediness are adapted according to online estimates of the learning progress, see Appendix A.5 for details. Average number of steps for successful transformations (bottom row in (a) and (c)) only shown if test success is $\geq 2\%$.

“forgets” how to deal with purely numerical coefficients between epochs $\tau \approx (1.5 \dots 3) \times 10^7$. Hence we raise the frequency of equations with purely numerical coefficients in the training data by increasing the probability p_0 of vanishing b_i (S3), which leads to a modest improvement on the purely numerical test sets again.

More consistent solutions for all types of test data sets are only achieved after changing to schemes with $a_i, b_i \in \mathbb{Q}$ (S4 and S5, dashed and dash-dot-dotted lines). In this way, we eventually obtain simultaneous success rates $\geq 86.5\%$ on equations with both purely numerical and mixed numerical/symbolic coefficients, meaning that the agent has essentially learned to deal with the problem types (6) and (7). Moreover, as before, the average number of steps to reach a solution, and thus the complexity of the learned strategies, is gradually reduced as training progresses.

3.3 Adversarial Task Generation

So far, we generated training tasks from fixed distributions and increased their complexity manually when the agent appeared to have mastered a class of problems. For equations involving symbolic coefficients, in particular, this required several adaptations of the training task distribution.

To streamline this process and to achieve an even more autonomous discovery of solution strategies, we introduce an adversarial learning scheme in the following. We train a second RL agent, the *generator*, simultaneously with the *solver* agent. In every episode, the generator creates a problem task, which is then passed to the solver. The generator operates in a similar environment as the solver (cf. Fig. 2), consisting of an equation (LHS and RHS) and a stack. Unlike the solver, however, the generator starts from a solution, i.e., an equation of the form (8), and tries to manipulate this equation such that it becomes unsolvable for the solver. To this end, the generator has access to the same set of actions plus an additional “submit” action to pass its current equation to the solver. After submission, the generator receives a positive reward r_{fool} if the solver fails to recover the solution, and no reward otherwise. In addition, a small penalty p_{step} is deducted for every step of the generator; see also Appendix A.6. This way, the generator is encouraged to find the simplest possible problem that overpowers the solver. As the solver’s capabilities improve, the generator will have to increase the problem complexity to keep pace.

Focusing on equations with purely numerical coefficients again first, we show the test performance of a single adversarially trained solver agent in Fig. 5a, utilizing the same sets of test equations as in Fig. 3a. Comparing these two sets of results, we observe that the adversarially trained solver achieves decent success rates faster than the agent learning from a fixed training distribution, although it ultimately fails to reach the same level of reliability (maximal success rate $\geq 74\%$ across both test sets). In Fig. 5b, we illustrate how the generator adapts its output as the solver becomes more successful: The blue bars show the relative frequency of classes of generated equations, whereas the orange bars correspond to the solver’s success on these equations. While those classes are only a coarse indicator of the equation difficulty, it is clearly visible how the diversity and complexity of the generator increases during training.

Finally, we turn to equations with mixed symbolic and numerical coefficients again, for which we show test performance results in Fig. 5c. Beginning with an adversarial learning scheme (AS1, solid lines), we observe some progress in the test success rates. Yet the eventually achieved success is not overly impressive, partly because the generator fails to explore the full spectrum of equations in the test data set. However, it turns out that the adversarially trained solver agent (AS1) forms an excellent basis for fixed-distribution training as in the previous subsection. Switching to such a scheme with equations involving symbolic and real-valued numerical coefficients after $t \approx 7.5 \times 10^6$ episodes (AS2, dashed lines), we eventually achieve success rates $\geq 94.2\%$ across all test data sets. Hence this agent outperforms the best agents found under the manual scheme (without adversarial pretraining, cf. Fig. 4) and learns to solve equations of all test types reliably. Moreover, no further adaptation of the training distribution or hyperparameters is necessary and the total training time is reduced considerably with adversarial pretraining.

4 Discussion

4.1 Related Studies

Machine-learning techniques have been adopted to tackle a variety of mathematical problems and tasks (He, 2023), from assisting with proofs and formulating conjectures (Kaliszyk et al., 2018; Bansal et al., 2019; Davies et al., 2021) to numerical solutions of algebraic (Liao and Li, 2022) and differential (Han et al., 2018) equations, representations of solutions for certain partial differential equations (Zhang and Bilige, 2019; Zhang and Li, 2022; Zhang et al., 2022), and efficient algorithms for high-dimensional arithmetic (Fawzi et al., 2022).

Among the more closely related applications, a particular example that also involves processing terms in a mathematically exact manner is symbolic regression. Here the goal is to deduce an analytical formula that describes a given data set, using a predefined set of available operations. Specific examples using machine learning include retrieving physical laws from measurements (Udrescu and Tegmark, 2020) and finding recurrence relations from example sequences (d’Ascoli et al., 2022).

As another example, Poesia et al. (2021) introduced a new reinforcement-learning scheme dubbed “contrastive policy learning” and subsequently applied it to find solutions of linear equations with integer coefficients. Besides the much smaller domain, the first major difference in their approach is that the agent does not need to discover inverse transformations by itself, but finds them among the available actions at each step. In our case, the agent must instead construct inverse operations through the stack, with the advantage of requiring fewer basic actions, but at the expense of additional elementary steps. The second major difference is that the focus of Poesia et al. (2021) is more on term simplification using basic algebraic axioms, a task that we have deliberately outsourced to SymPy (see last paragraph of Sec. 2.4). Hence both the motivation and the actual learning task are quite different. Indeed, one of the main conclusions of Poesia et al. (2021) is that deep Q -learning—as we adopt it here—fails to find reliable solution strategies within their framework.

Yet another important example of standard CAS functionality, symbolic integration, was tackled by machine-learning methods by Lample and Charton (2020). Here the task is to find an indefinite integral of a given mathematical expression. Their approach uses supervised learning of so-called sequence-to-sequence models, which are commonly adopted for natural language processing. Similarly to math-text problems (see below), and contrary to the philosophy of our approach, the machine does not discover the underlying elementary transformation rules on its own, but is trained on a large data set of exemplary function–integral pairs to predict an integral (output) from a function (input). The model achieves impressive success rates, though some reservations regarding the test set and generality apply (Davis, 2019; Ornes, 2020). Furthermore, the machine’s “reasoning” behind successful (or failed) integration attempts remains intransparent to humans.

A previously studied task which often involves aspects of equation solving are math-text exercises, i.e., formulations of mathematical problems in natural language. Besides the actual arithmetic, the challenge here is to extract the abstract math problem from the verbal description. This type of problem has been tackled most successfully with language models (Wei et al., 2022; Drori et al., 2022; Lewkowycz et al., 2022; Bubeck et al., 2023; Wolfram, 2023a), i.e., neural networks specialized in natural language processing. The models are trained on a huge corpus of human-authored texts and, when primed for math and science

reasoning, exemplary problem sets and solutions. Their solution strategies thus imitate human approaches: The neural network generates a textual output which it estimates to be the most likely solution for the given question based on the training corpus, with remarkable albeit far from perfect success rates. By construction, this method is unlikely to succeed when applied to previously unexplored domains where human-solved examples are unavailable.

Another major caveat is that language models will always produce an answer and sell it seemingly convincingly, but there is actually no guarantee for correctness of the answer itself nor of the underlying reasoning. As an illustration, we asked ChatGPT 3.5 (OpenAI, 2024) to consider some of the test problems used in our analysis, notably the one from Fig. 3d, $-\frac{1}{5} + \frac{3}{4}x = \frac{5}{8} + 2x$. ChatGPT arrives at a wrong “solution”, $x = -9$, because in one step of the “derivation”, the two sides of the equation are multiplied by different constants (ChatGPT Example Chat). Details and a screenshot of the full chat record are provided in Appendix B. We emphasize that the above equation is of the simplest type considered by us, involving purely numerical, real-valued coefficients. Of course, ChatGPT does correctly answer some other examples of similar equations and other (future) large language models may achieve even higher success rates, but the point is that there is no guarantee of obtaining the correct answer – one can never be sure unless one carefully scrutinizes their line of reasoning. A partial remedy for this hallucination problem is to “outsource” the actual logic, for instance by translating the mathematical question into a query to specialized software such as a CAS (Wolfram, 2023a). In this case, however, the actual solution strategy must have been known and algorithmically implemented a priori by humans. By contrast, our present approach does not presume human knowledge about solution strategies, with the effect that it may fail to produce a solution, but it will never generate a wrong answer.

4.2 Conclusions and Outlook

Our work explores a new way to adopt machine learning for exact mathematics, a domain that has proved to be troublesome for traditional approaches. It can be seen as a first step towards general machine-learning strategies to discover laws of mathematical reasoning and deduction. Specifically, we devised a neural-network-powered RL agent that acquires the capability of solving linear equations by composing elementary equivalence transformations. It builds on established rules for handling mathematical terms and discovers autonomously how such manipulations can be adopted to master a new domain. In some sense, this situation is similar to a middle-school student who already knows the rules of basic algebra, but still needs to learn about the concept of equations and how to solve them. More generally, mathematical research can be seen as a gradual exploration of how axioms and previous insights can be combined to reveal something nontrivial that was not immediately apparent from the original components. Here we showcase a strategy for how machines can be utilized for this endeavor. Our demonstration uses the arguably simple example of solving linear equations. However, the proposed scheme based on a symbolic stack calculator can be directly extended to other types of algebraic equations by a suitable adaptation of the available operations, and we expect that the idea of having an RL agent explore a suitable

“theory space” can prove itself effective in other computer-algebra domains as well and aid mathematical research in general.

A primary design principle of our approach was to provide an unbiased setting in which the agent explores how to solve the task without reference to what humans may perceive as the best strategy. Hence we deliberately avoided certain techniques that could have accelerated the learning process, but introduce a human bias, such as supervised (pre)training, intermediate rewards, or preselected inverse transformations. Crucially, once the machine finds a successful recipe, its strategy remains comprehensible to humans thanks to the composition from simple elementary transformations, such that humans can subsequently learn it from the machine. In an educational context, for instance, such an RL agent could be used to offer hints for the next step in an exercise to students or complete step-by-step solutions.

At present, our approach is limited to the simple example of linear algebraic equations. Thanks to the ability to deal with symbolic coefficients, systems of linear and even simple nonlinear equations can also be solved in principle. However, as the number of variables increases, the term size will grow significantly, too, which will make it harder and computationally more costly to process terms and train the agent.

It merits further study to extend the solution capabilities to other types of equations and inequalities. This will bring along additional challenges like problems with multiple solutions, problems that cannot be solved symbolically in closed form, as well as the need for more computing resources due to larger term sizes and action spaces. Furthermore, it will be of both fundamental and practical interest to develop similar schemes for other types of computer algebra problems, e.g., term simplification, symbolic integration, limits and series representations, and eventually tackle tasks that are not amenable using presently available software.

Acknowledgements

This work was supported by KAKENHI Grant No. JP22H01152 from the Japan Society for Promotion of Science.

Appendix A. Implementation Details

A.1 Task Sampling

In the first part of this work (Secs. 3.1 and 3.2), sample problems during training are generated by sampling the coefficients a_i, b_i in Eqs. (6)–(7) randomly and independently from fixed probability distributions. Let $U_n^{\mathbb{N}}$ denote the uniform distribution on $\{1, 2, \dots, n\}$ and $U_n^{\mathbb{Z}}$ the uniform distribution on $\{-n, -n+1, \dots, n\}$. We then have: for $a_i \in \mathbb{Z}$, $a_i \sim U_{10}^{\mathbb{Z}}$; for $a_i \in \mathbb{Q}$, $a_i = p/q$ with $p \sim U_{50}^{\mathbb{Z}}$, $q \sim U_{10}^{\mathbb{N}}$; for $a_i \in K + iK$, $a_i = \alpha_{\text{re}} + i\alpha_{\text{im}}$ with α_{re} and α_{im} independent and randomly drawn from $K = \mathbb{Z}$ or \mathbb{Q} according to the aforementioned schemes. The numbers b_i multiplying the symbolic constant c in type (7) are set to zero with probability p_0 and otherwise sampled from the same distribution as the a_i . The fixed test data sets (cf. Appendix D) are generated from the same distributions.

In the second part of this work (Sec. 3.3), training tasks are generated by an additional RL agent that adapts to the capabilities of the solver as outlined in Sec. 3.3. The solutions

from which the generators start are drawn randomly as $x = a_1$ (AR, Fig. 5a,b) or $x = (a_1 + b_1c)/(a_2 + b_2c)$ (AS1, Fig. 5c) with $a_i, b_i \in \mathbb{Q}$ distributed as before.

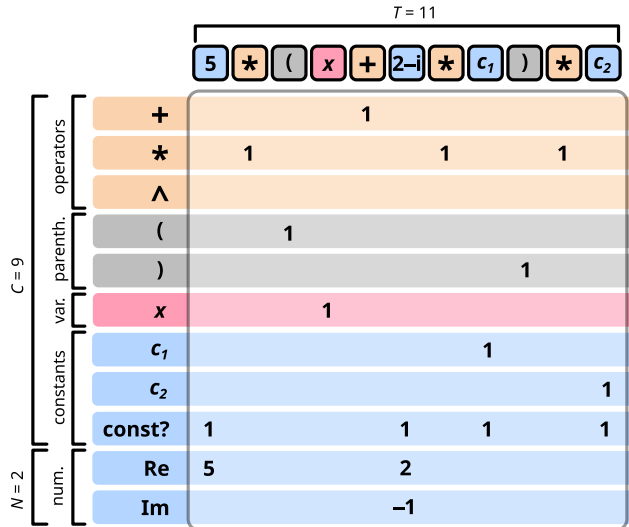


Figure 6: Illustration of the state-tensor representation using feature planes for the example term $5x(x + (2 - i)c_1)c_2$. Every term is mapped to a $(C + N) \times T$ tensor, whose columns correspond to the elementary units (operators, parentheses, variables, numbers) of the expression. The C character rows hold binary indicators of whether a specific (type of) symbol occurs in the respective position of the term. The N number rows encode the floating-point values of numerical constants. Empty entries correspond to the value zero. A full state representation consists of $S + 2$ such term tensors (left- and right-hand sides of the equation as well as the stack entries).

A.2 State Encoding

To feed the observed state s into the neural network $f_\theta(s)$ for the Q function, we need to translate s into a suitable representation. We recall that the state consists of $S + 2$ terms (stack, LHS, RHS), each of which can contain up to T elementary units, cf. Fig. 2a. We encode each of these terms in a feature plane as illustrated in Fig. 6, which is a $(C + N) \times T$ matrix. Its T columns correspond to the term’s elementary units (in standard infix notation, see also below), and the rows encode the contents of those units. The first C rows contain binary indicators for whether or not the unit is of a specific type. There are O_{st} rows for the supported operators (here: $+$, $*$, \wedge), two rows for the left and right parentheses, one row for the variable x , and one row for each additional symbolic constant. Furthermore, there is one row to indicate whether the unit contains a constant (numerical or symbolic). Finally, there are N additional rows to encode the floating-point values of the numerical constants ($N = 1$ for real-valued coefficients, $N = 2$ for possibly complex-valued coefficients). Hence the overall input to the neural network is an $(S + 2) \times (C + N) \times T$ -dimensional tensor, and

its output is an A -dimensional tensor where $A = 2T + O_{\text{eq}} + C_{\text{num}} + O_{\text{st}}$ is the total number of available actions (cf. Fig. 2b). In our examples, the input and output dimensions range from 280 to 1071 and 18 to 45, respectively, cf. Tables 3 and 4 below.

The state representation passed on to the neural network is based on the standard infix notation of mathematical expressions, meaning that a term whose top-level operator takes multiple arguments (such as $+$, $*$) is expressed by interleaving the arguments with copies of the operator symbol (“ $x + c + 1$ ”). A more natural encoding of mathematical terms is an expression tree with the nodes corresponding to the operators and the leaves representing variables and numbers, and this is also the format of our internal (SymPy-based) representation. It clearly maps out the hierarchy and priorities of the operations and avoids the need for parentheses and/or implicit operator precedence rules, but does not have a natural embedding into the layout of network tensors. An alternative to the infix representation is a prefix notation, which avoids operator precedence rules and parentheses, provided that the number of arguments is fixed for each operator. However, the latter condition introduces an artificial evaluation hierarchy, and the prefix notation can lead to very nonlocal representations in the sense that arguments appear far away from their operators. Altogether, we could not identify a clear practical advantage of either prefix or infix notation and thus stuck with the latter, which has the additional advantage of familiarity and thus better interpretability by humans.

For the floating-point representation of (the real and imaginary parts of) numerical constants in the N number rows of the state tensor (cf. Fig. 6), we rescale and cap them to obtain typical values of order unity for numerical stability. Concretely, for (the real or imaginary part of) a coefficient a , the corresponding entry of the state tensor is set to $a/100$ if $|a| \leq 500$ and otherwise causes a numerical overflow.

A.3 Network Architecture and Training Algorithm

We adopt neural networks f_θ with three (four) hidden layers of 8000, 4000, 2000 (16 000, 8000, 4000, 2000) units for the problems of type (6) (type (7)). We use the standard ReLU activation function ($\sigma(x) = \max\{0, x\}$) as our nonlinearity for all layers except the last one, which is linear.

We update the network parameters θ_τ according to the double deep Q -learning scheme (Hasselt et al., 2016) with experience replay (Mnih et al., 2015): In every epoch τ , the agent explores p steps in the current environment following an ε -greedy policy with respect to its present Q -function estimate $Q(s, a) = [f_{\theta_\tau}(s)]_a$, meaning that the highest-valued action is chosen with probability $1 - \varepsilon$ and a random action otherwise. Invalid actions are masked (cf. Appendix A.4) and the (non)greediness ε is gradually decreased with the training progress (cf. Appendix A.5). The observed 4-tuples (s_t, a_t, r_t, s_{t+1}) of explored transitions are stored in a replay memory with maximum capacity M . (Note that t denotes the time within the current episode of the RL environment, i.e., the number of actions taken by the agent since the current task was assigned. It should not be confused with the training time τ , which counts the total number of parameter updates/training epochs.)

Thereafter, we sample a batch of B transitions $\omega := (s, a, r, s')$ uniformly at random from the replay memory and calculate the current estimate of $Q(s, a)$ (LHS of the Bellman equation (5)) for all state-action pairs (s, a) in the batch by evaluating the network function f_{θ_τ} . To obtain a sufficiently decorrelated estimate of the RHS of the Bellman equation (5),

its Q values are estimated from a second *target network*, whose parameters $\hat{\theta}_\tau$ are aligned with the parameters θ_τ of the *online network* only every $\hat{\tau}$ epochs. The squared residual of Eq. (5) associated with the transition ω is thus

$$\ell_\theta(\omega) := ([f_\theta(s)]_a - r - \gamma[f_{\hat{\theta}}(s')]_{a'})^2, \quad (9)$$

where $a' := \arg \max_a [f_\theta(s')]_a$ and, by convention, $f_{\hat{\theta}}(s') \equiv 0$ if s' is a terminal state (solved or invalid). Our loss function is the mean over those residuals for all transitions in the batch, $L_\theta := \frac{1}{B} \sum_\omega \ell_\theta(\omega)$. The online-network parameters θ_τ are then updated using gradient descent with learning rate η , $\theta_{\tau+1} := \theta_\tau - \eta \nabla_\theta L_{\theta_\tau}$.

Our actual implementation relies on the PyTorch library (Paszke et al., 2019). The relevant hyperparameters and their values in our experiments are summarized in Tables 1–4 below.

A.4 Invalid Action Masking

For training and inference, actions that are invalid in a given state are masked, i.e., they are excluded from the available options. Concretely, this means that the greedy policy chooses the action with the highest $Q(s_t, a) = [f_\theta(s_t)]_a$ among the valid actions a in the current state s_t , and the random policy uniformly selects one of these valid actions. Invalid actions are:

- “copy LHS n (RHS n) to stack” if the term size of LHS (RHS) is less than n . For example, the term $2+4*x$ has five elementary units, so any copy actions for positions beyond 5 are masked;
- “apply \mathbf{f} on stack” if \mathbf{f} requires n arguments, but the number of stack entries is less than n ;
- “apply \mathbf{f} on equation” if \mathbf{f} requires n arguments from the stack, but the number of stack entries is less than n ;
- multiply the equation by zero;
- “apply $\hat{}$ on stack” with arguments a and b (i.e. a^b) if $a = 0$ or $b \notin \mathbb{Z} \setminus \{0\}$.

Note that the last type of action is not mathematically invalid, but can lead to ambiguities (e.g., regarding the sign of a variable when $b = \frac{1}{2}$) that would require special care. Since transformations of this kind are not needed within the domain of equations under study, we exclude them to avoid such subtleties.

For the generator agent within the adversarial learning approach, the “submit” action is masked if “LHS = RHS” is not a linear equation.

A.5 Greediness and Learning-Rate Schedules

During training, we dynamically adjust the (non)greediness of our ε -greedy policy with the training progress. We use two different schemes: (i) exponentially decaying schedules of the general form

$$\varepsilon(\tau) = (\varepsilon_i - \varepsilon_f) e^{-\tau/T_\varepsilon} + \varepsilon_f, \quad (10)$$

which interpolate between the initial value ε_i ($\tau = 0$) and asymptotic final value ε_f ($\tau \rightarrow \infty$), where τ is the training time (number of parameter updates); (ii) adaptive schedules of the form

$$\varepsilon(s) = (\varepsilon_i - \varepsilon_f)(1 - s)^{\alpha_\varepsilon} + \varepsilon_f, \quad (11)$$

where $s \in [0, 1]$ is an online estimate of the current agent capabilities and ε_i (ε_f) is the maximum (minimum) value. For solver agents, s is the fraction of successfully solved equations within the last 100 episodes. For generator agents, s is the minimum of the success rate to generate valid equations and the failure rate of the solver within the last 100 episodes. The values of ε_i , ε_f , T_ε , and α_ε in our experiments are listed in Tables 3 and 4.

The learning rates are either kept fixed for a specific training configuration,

$$\eta(\tau) = \eta = \text{const}, \quad (12)$$

or adjusted dynamically similarly as in (11),

$$\eta(s) = (\eta_i - \eta_f)(1 - s)^{\alpha_\eta} + \eta_f. \quad (13)$$

Here s is the same online quality estimate as before. The adopted values in the experiments are listed in Tables 3 and 4, too.

A.6 Rewards

Solver agents. As explained in Sec. 2.4, the total reward when an equation is solved is given by the success reward r_{slv} , reduced by penalties for remaining stack entries (p_{st}) and assumptions about unknowns (p_{as}). The idea behind issuing no rewards for intermediate steps and only for final states (solved equations) is to avoid any human bias about what kinds of operations might be perceived as expedient or wasteful. The penalties serve to encourage concise strategies and thus to reduce the computational complexity of the learned solution algorithms. Our explicit formula to calculate the final reward is

$$r = r_{\text{slv}} - \frac{n_{\text{st}}}{S} p_{\text{st}} - n_{\text{as}} p_{\text{as}}, \quad (14)$$

where n_{st} is the number of stack entries in the final state, S the stack capacity, and n_{as} the number of assumptions. Any terms remaining on the stack after a solution has been found indicate that some transformation steps were unnecessary. The stack penalty thus helps to avoid such superfluous steps. Assumptions are added whenever an operation involves a variable (x or c) and is not generally valid for all real or complex values of this variable. For example, when the action “apply \sim on stack” is selected with base $c + 1$ and exponent -1 , the assumption “ $c + 1 \neq 0$ ” is added. As another example, when choosing the action “apply $*$ on equation” with the stack argument $2x - 3$, the assumption “ $2x - 3 \neq 0$ ” is added. If the same assumption is required twice, it will only be added once. Note that assumptions cannot generally be avoided if the equation involves variables besides the unknown to solve for, but the agent should be encouraged to find transformations that require as few of them as possible.

To further discourage pointless manipulations and auxiliary calculations, we also consider the possibility of issuing a negative reward r_{so} in case of a “stack overflow,” i.e., when

the agent chooses to push a term to the stack even though the latter already holds S terms. (The action is still carried out, with the result that the lowest entry on the stack, which had been there the longest, is discarded.)

Generator agents. For generator agents as introduced in Sec. 3.3, the total reward after the “submit” action is given by

$$r = \begin{cases} 0 & \text{if solver found solution} \\ r_{\text{fool}} & \text{otherwise} \end{cases} - \frac{n_{\text{st}}}{S} p_{\text{st}} - n_{\text{as}} p_{\text{as}}. \quad (15)$$

Here the stack and assumption penalties are handled like for the solver agents.

After all other actions, a negative reward (step penalty) is issued to encourage fast submission:

$$r = -p_{\text{step}}. \quad (16)$$

The concrete values for rewards and penalties in the numerical experiments are listed in Tables 3 and 4.

A.7 Term Processing

As mentioned in the main text, our RL environment automatically simplifies mathematical expressions when updating its state. This includes the following steps in order:

- if constants can be complex-valued numbers or symbolic, call SymPy’s `expand` function;
- if constants can be symbolic, call SymPy’s `cancel` function. Without doing so, spurious dependencies on the variable can sometimes remain and the environment can fail to detect that an equation has been solved. E.g., the simplification $[-f(x)][f(x)]^{-1} \rightarrow -1$ may fail;
- call SymPy’s `collect` function to collect terms in the variable to be solved for, e.g., $3x + 2cx - 1 \rightarrow (3 + 2c)x - 1$;
- group (and simplify if possible) numerical arguments in commutative (sub)terms, e.g., $1 + x + \frac{3}{2} + 2c + \sqrt{2} \rightarrow (\frac{5}{2} + \sqrt{2}) + x + 2c$;
- randomly shuffle the order of operands in commutative (sub)terms. This improves training stability and generalization. It also entails that the environment is nondeterministic.

We emphasize that we do not use SymPy’s heuristic `simplify` function as it is computationally quite expensive and the results can vary depending on term structure, variable names, etc.

Appendix B. Equation solving with ChatGPT

As discussed in Sec. 4, a conceptual advantage of our method compared to other approaches, notably large language models (LLMs), is that our reinforcement-learning agent cannot

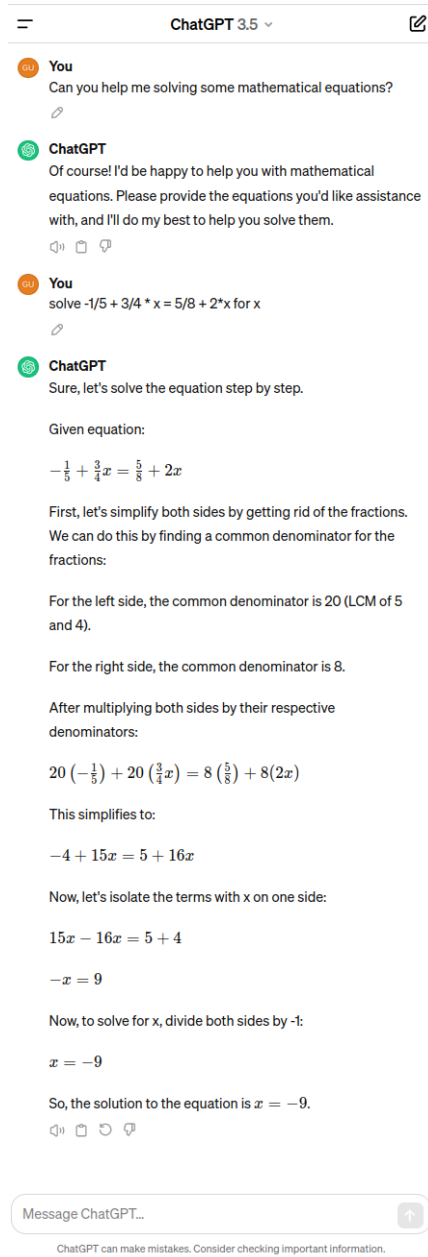


Figure 7: Screenshot of the chat record asking ChatGPT 3.5 to solve the example from Fig. 3, $-\frac{1}{5} + \frac{3}{4}x = \frac{5}{8} + 2x$. Accessed on March 23, 2024; share link: <https://chat.openai.com/share/469a5885-3e37-404c-bd11-fca52b00a8eb>. The screenshot shows the full record after starting a new chat, i.e., all prompts are shown.

hallucinate because the exploration domain is restricted to mathematically valid transformations. As an illustration of hallucination effects in LLMs, we confronted OpenAI’s publicly available ChatGPT with the example problem from Fig. 2d. The full chat record is shown in Fig. 7 and can also be accessed from this URL: <https://chat.openai.com/share/469a5885-3e37-404c-bd11-fca52b00a8eb>. We emphasize that this is not a cherry-picked example. For example, we also tested ChatGPT on the first ten equations from our `lin-crat-N1000` dataset (cf. Appendix D), of which ChatGPT correctly solved six equations (see <https://chat.openai.com/share/bc879182-53ab-4ff4-aab4-4519ba711e7f>).

We also emphasize once more that ChatGPT was not explicitly trained to solve these types of equations, hence it would be presumptuous to claim that our model is superior in any meaningful way. The mere purpose of these examples is to point out the caveats that come with employing language models for such mathematical problems, namely the tendency to fabricate arguments that look superficially consistent, but contain logical flaws that can be hard to detect. Thus it is important to explore alternative learning environments and architectures that do not suffer from these issues, and this was one of our design goals for the framework proposed here.

Appendix C. Hyperparameters

Hyperparameters characterizing the RL environment and the training algorithm are summarized in Tables 1 and 2, respectively. The concrete values adopted in the numerical experiments are listed in Tables 3 and 4. We did not specifically optimize the environment hyperparameters (Table 1). For the training hyperparameters (Table 2), we usually explored several different training schemes, mostly focusing on the learning rate η , the greediness ε , the update frequencies p and $\hat{\tau}$ of the online and target networks, and, to a lesser extent, the discount rate γ and the batch size B .

We did not perform a systematic grid search to find globally optimal parameters due to the large number of hyperparameters and the inherent randomness of the training process, which may entail significant performance differences between training runs with the same parameters due to the instability of deep Q -learning (Sutton and Barto, 2018; van Hasselt et al., 2018; Wang and Ueda, 2022). However, a more quantitative account of the dependence on the various hyperparameters is provided in Tables 5–16, where we show success rates for variations of the models from Figs. 3–5 (see also Tables 3 and 4). Note that the success rates in Tables 5–13 (non-adversarial framework) are based on the ε -greedy policy and smaller, random test sets of 500 equations drawn from the same distributions as used for training. Hence the results can vary slightly compared to the analysis shown in Figs. 3–4, which used a greedy policy ($\varepsilon = 0$) and fixed sets of test equations. Furthermore, the quoted best success rates might be surpassed during further training with the respective hyperparameters.

Table 1: Constants characterizing the reinforcement-learning environment.

Symbol	Name	Description
A	action count	number of actions available to the RL agent, output dim. of the neural network
C	character rows	number of rows to indicate the type of elementary term units
C_{num}	constants count	number of numerical constants that can be pushed directly onto the stack
N	number rows	number of rows to indicate values of numerical constants
O_{eq}	equation operations	number of operations that can be performed on the equation
O_{st}	stack operations	number of operations that can be performed on the stack
S	stack size	max. number of terms on the stack
T	term size	max. number of elementary units of any term

Table 2: Hyperparameters of the neural network architecture and deep Q -learning algorithm.

Symbol	Name	Description
H	hidden layers	number of hidden layers
M	replay capacity	number of (s_t, a_t, r_t, s_{t+1}) transitions in the replay memory
p	online update frequency	number of exploration steps per parameter update of the online network
$\hat{\tau}$	target update frequency	number of online parameter updates per update of the target network
$\hat{\varepsilon}$	target update greediness	$\hat{\theta} \leftarrow (1 - \hat{\varepsilon})\hat{\theta} + \hat{\varepsilon}\theta$, default: $\hat{\varepsilon} = 1$
γ	discount rate	see Eq. (4) of the main text
ε	greediness	probability for random action selection during training
$\varepsilon_i, \varepsilon_f$	max./min. greediness	see Eqs. (10) and (11)
T_ε	greediness decay time	see Eq. (10)
α_ε	greediness exponent	see Eq. (11)
η	learning rate	see below Eq. (9) of the main text and Eqs. (12) and (13)
η_i, η_f	max./min. learning rate	see Eq. (13)
α_η	learning rate exponent	see Eq. (13)
μ	momentum	default: $\mu = 0$
B	batch size	number of replay transitions used for gradient estimates
t_{max}	maximum steps	maximum number of elementary steps (actions) for each problem before aborting the episode
r_{slv}	success reward	maximal reward upon solving an equation, see Eq. (14)
r_{fool}	fooling reward	maximal generator reward when fooling the solver, see Eq. (15)
r_{so}	stack overflow penalty	(negative) reward for pushing terms on the stack beyond its capacity
p_{st}	stack penalty	penalty for remaining stack entries on success, see Eqs. (14) and (15)
p_{as}	stack penalty	penalty for assumptions on success, see Eq. (14) and (15)

Table 3: Parameter values of the solver networks in the numerical experiments, cf. Figs. 3–5 of the main text

Symbol	Values												
	R1	R2	C1	C2	S1	S2	S3	S4	S5	AR	AS1	AS2	
A (output dim.)	18		19		42					20		44	
C	7		7		8					7		8	
C_{num}	3		4		3					4		4	
N	1		2		1					2		2	
O_{eq}	2		2		2					3		2	
O_{st}	3		3		3					3		3	
S	5		5		5					5		4	
T	5		5		17					5		17	
input dim.	280		350		1071					315		1020	
total parameters	42 290 018		42 852 019		185 250 042					44 555 020		184 438 044	
H	3		3		4					4		4	
M	5×10^5		5×10^5		5×10^5					5×10^5		5×10^5	
p	4		4		4	4	8	4	4	8		8	
$\hat{\tau}$	100		100		100					100		100	
γ	0.9		0.9		0.9					0.9		0.9 0.95	
ε	Eq. (10)		Eq. (10)		Eq. (10)					Eq. (11)		Eq. (11)	
ε_i	1	0.3	1	0.3	1	0.3	0.6	0.2	0.2	0.5		0.5	0.3
ε_f	0.1	0.05	0.1	0.1	0.1	0.1	0.1	0.05	0.01	0.1		0.1	
T_ε	$5M$		$5M$		$5M$					$5M$		$5M$	
α_ε	—		—		—					1		1	
η	0.05	0.01	0.05	0.01	0.05	0.05	0.01	0.05	0.01	Eq. (13)		Eq. (13)	
η_i	—		—		—					0.05		0.05	
η_f	—		—		—					0.005		0.005	
α_η	—		—		—					0.5		0.5	
B	128		128		128					128		128	
t_{max}	100		100		100					100		100	
r_{siv}	3		3		3					3		3	
r_{so}	−0.25		−0.25		−0.25					0		0	
p_{st}	1		1		1					1		1	
p_{as}	0.25		0.25		0.25					0.25		0.25	
test data set	1000 equations		1000 equations		10 000 equations					10 000 equations		10 000 equations	

Table 4: Parameter values of the generator networks in the numerical experiments, cf. Fig. 5 of the main text

Symbol	Values	
	AR	AS1
A (output dim.)	21	45
C	7	8
C_{num}	4	4
N	2	2
O_{eq}	3	2
O_{st}	3	3
S	5	4
T	5	17
input dim.	315	1020
total parameters	44 556 021	184 440 045
H	4	4
M	5×10^5	5×10^5
p	8	8
$\hat{\tau}$	100	100
γ	0.9	0.9
ε	Eq. (11)	Eq. (11)
ε_i	0.5	0.5
ε_f	0.1	0.1
T_ε	—	—
α_ε	1	1
η	Eq. (13)	Eq. (13)
η_i	0.01	0.01
η_f	0.001	0.001
α_η	0.5	0.5
B	128	128
t_{max}	100	100
r_{fool}	3	3
r_{so}	0	0
p_{st}	1	1
p_{as}	0.25	0.25

Table 5: Best test success rates on random test sets of 500 equations of type (6) with $a_i \in \mathbb{Z}$ (cf. Appendix A.1) for hyperparameter variations of model R1 (cf. Fig. 4 of the main text and Table 3). First row is the reference (R1), subsequent rows show variations; hyperparameter values are only shown if they differ from the reference.

	hidden layers	M	Hyperparameters								success rate
			p	$\hat{\tau}$	$\hat{\varepsilon}$	γ	T_ε	η	μ	B	
R1 (ref.)	8000, 4000, 2000	5×10^5	4	100	1	0.9	5M	0.05	0	128	91 %
							10M				78 %
	4000, 2000, 1000	1×10^4	1				10M				10 %
	4000, 2000, 1000	5×10^4	1				10M				77 %
	4000, 2000, 1000	2×10^5	1				10M				80 %
	4000, 2000, 1000	1×10^5	1				10M			32	15 %
	4000, 2000, 1000	1×10^5	1				10M				42 %
	4000, 2000, 1000	1×10^5	1				10M				93 %
	4000, 2000, 1000	1×10^5	1				10M	0.02		512	15 %
	4000, 2000, 1000	1×10^5	1				20M				38 %
	4000, 2000, 1000	1×10^5	1				20M	0.02		512	15 %
	4000, 2000, 1000	1×10^5	1				10M			512	10 %
	4000, 2000, 1000	1×10^5	1	10	0.1		10M				20 %
	4000, 2000, 1000	1×10^5	1	10	0.01		10M				85 %
	4000, 2000, 1000	1×10^5	1	10	0.01		10M		0.1		54 %
	4000, 2000, 1000	1×10^5	1	1000			10M				10 %
	4000, 2000, 1000	1×10^5	1			0.95	10M				15 %
	4000, 2000, 1000	1×10^5	2				10M				49 %
	4000, 2000, 1000	1×10^5	8				10M				15 %
	4000, 2000, 1000	1×10^5	1				10M	0.01	0.1		15 %
	4000, 2000, 1000	1×10^5	1				20M		0.1		5 %
	4000, 2000, 1000	1×10^5	1				10M		0.1		64 %
	4000, 2000, 1000	1×10^5	1				10M		0.2		83 %

Table 6: Best test success rates on random test sets of 500 equations of type (6) with $a_i \in \mathbb{Z} + i\mathbb{Z}$ (cf. Appendix A.1) for hyperparameter variations of model R2.

	Hyperparameters		success rate
	$\hat{\varepsilon}$		
R2 (ref.)	1		97 %
	0.1		71 %

Table 7: Best test success rates on random test sets of 500 equations of type (6) with $a_i \in \mathbb{Z}$ (cf. Appendix A.1) for hyperparameter variations of model C1.

	Hyperparameters				success rate
	p	T_ε	η	μ	
C1 (ref.)	4	5M	0.05	0	90 %
	1				88 %
		10M			88 %
			0.01	0.2	8 %

Table 8: Best test success rates on random test sets of 500 equations of type (6) with $a_i \in \mathbb{Z} + i\mathbb{Z}$ (cf. Appendix A.1) for hyperparameter variations of model C2.

	Hyperparameters		success rate
	ε_i	T_ε	
C2 (ref.)	0.3	5M	98 %
	0.6		93 %
		10M	85 %

Table 9: Best test success rates on random test sets of 500 equations of type (7) with $a_i, b_i \in \mathbb{Z}$, $a_0 = b_0 = a_3 = b_3 = 0$ or $a_1 = b_1 = a_2 = b_2 = 0$, and $p_0 = 0$ (cf. Appendix A.1) for hyperparameter variations of model S1.

	Hyperparameters						success rate
	hidden layers	p	ε_i	T_ε	η		
S1 (ref.)	16 000, 8000, 4000, 2000	4	1	5M	0.05		93 %
			8				93 %
					10M		
		8000, 4000, 2000		0.6			90 %
		8000, 4000, 2000		0.6	10M	0.01	3 %
		8000, 4000, 2000		0.6		0.01	5 %

Table 10: Best test success rates on random test sets of 500 equations of type (7) with $a_i, b_i \in \mathbb{Z}$ and $p_0 = \frac{1}{2}$ (cf. Appendix A.1) for hyperparameter variations of model S2.

	Hyperparameters					success rate	
	p	ε_i	ε_f	T_ε	η		
S2 (ref.)	4	0.3	0.1	10M	0.05	49 %	
		8				37 %	
			0.6			36 %	
			0.9			5 %	
			0.1	0.05		0.01	34 %
				10M			6 %

Table 11: Best test success rates on random test sets of 500 equations of type (7) with $a_i, b_i \in \mathbb{Z}$ and $p_0 = \frac{2}{3}$ (cf. Appendix A.1) for hyperparameter variations of model S3.

	Hyperparameters			success rate
	p	ε_i	η	
S3 (ref.)	8	0.6	0.01	78 %
	4			74 %
	4	0.3		75 %
		0.3	0.02	57 %
		0.3	0.05	71 %
	4	0.3	0.02	75 %
	4	0.3	0.05	66 %

Table 12: Best test success rates on random test sets of 500 equations of type (7) with $a_i, b_i \in \mathbb{Q}$ and $p_0 = \frac{2}{3}$ (cf. Appendix A.1) for hyperparameter variations of model S4.

	Hyperparameters			success rate
	p	ε_i	η	
S4 (ref.)	4	0.2	0.05	80 %
	8			77 %
			0.01	75 %
	8		0.01	70 %
	8	0.6	0.01	30 %

Table 13: Best test success rates on random test sets of 500 equations of type (7) with $a_i, b_i \in \mathbb{Q}$ and $p_0 = \frac{2}{3}$ (cf. Appendix A.1) for hyperparameter variations of model S5.

	Hyperparameters				success rate
	p	$\hat{\varepsilon}$	ε_i	ε_f	
S5 (ref.)	4	1	0.2	0.01	85 %
	8				90 %
		0.1			83 %
			0.1		81 %
				0.05	87 %
	8			0.05	83 %
			0.4	0.05	84 %

Table 14: Best test success rates on the test data set of 10 000 equations of type (6) with $a_i \in \mathbb{Q}$ (cf. Appendix A.1) for hyperparameter variations of model AR.

	generator hyperparameters		solver hyperparameters				success rate
	ε_i	η_i	p	γ	ε_i	η_f	
AR (ref.)	0.5	0.01	8	0.9	0.5	0.005	74 %
			4	0.95			67 %
		0.05				0.001	3 %
	0.8				0.8		86 %
						56 %	

Table 15: Best test success rates on the test data set of 10 000 equations of type (7) with $a_i, b_i \in \mathbb{Q}$ and $p_0 = \frac{2}{3}$ (cf. Appendix A.1) for hyperparameter variations of model AS1.

	Hyperparameters		success rate
	p	γ	
AS1 (ref.)	8	0.9	16 %
		0.95	5 %
	4		< 1 %
	4	0.95	< 1 %

Table 16: Best test success rates on the test data set of 10 000 equations of type (7) with $a_i, b_i \in \mathbb{Q}$ and $p_0 = \frac{2}{3}$ (cf. Appendix A.1) for hyperparameter variations of model AS2.

	Hyperparameters					success rate
	p	γ	ε_i	η_f	α_η	
AS2 (ref.)	8	0.95	0.3	0.005	0.5	99 %
		0.9		0.01		98 %
	4	0.9	0.5			59 %
		0.9	0.5		1	61 %

Appendix D. Data Sets

The archive `sm_datasets.zip` contains the following files:

- `lin-cint-N1000.txt`, `lin-cint-N10000.txt`: Test data sets of 1000 and 10 000 equations with integer coefficients (main text Eq. (6), $a_i \in \mathbb{Z}$).
- `lin-crat-N1000.txt`, `lin-crat-N10000.txt`: Test data sets of 1000 and 10 000 equations with rational coefficients (main text Eq. (6), $a_i \in \mathbb{Q}$).
- `lin-ccpxint-N1000.txt`, `lin-ccpxint-N10000.txt`: Test data sets of 1000 and 10 000 equations with complex-integer coefficients (main text Eq. (6), $a_i \in \mathbb{Z} + i\mathbb{Z}$).
- `lin-ccpxrat-N1000.txt`, `lin-ccpxrat-N10000.txt`: Test data sets of 1000 and 10 000 equations with complex-rational coefficients (main text Eq. (6), $a_i \in \mathbb{Q} + i\mathbb{Q}$).
- `lin-cint+0.5sym1-N10000.txt`: Test data set of 10 000 equations with symbolic and integer numerical coefficients (main text Eq. (7), $a_i, b_i \in \mathbb{Z} + i\mathbb{Z}$, $p_0 = \frac{1}{2}$, cf. Methods).
- `lin-crat+0.33sym1-N10000.txt`: Test data set of 10 000 equations with symbolic and rational numerical coefficients (main text Eq. (7), $a_i, b_i \in \mathbb{Q} + i\mathbb{Q}$, $p_0 = \frac{2}{3}$, cf. Methods).
- `fig3a.txt`, `fig3b.txt`, `fig4.txt`, `fig5a.txt`, `fig5c.txt`: Source data of figures in the main text. Space-separated test success rates (`test_success_*` columns) and average number of steps (`avg_steps_*` columns) for all training and test configurations, cf. the headers in each file.
- `fig5b.txt`: Source data of Fig. 5b in the main text. Space-separated generator frequencies (`generated('...')`) and solver success rates (`solved('...')`) for all equation classes, cf. the file’s header.

References

- OpenAI: Marcin Andrychowicz, Bowen Baker, Maciek Chociej, Rafal Józefowicz, Bob McGrew, Jakub Pachocki, Arthur Petron, Matthias Plappert, Glenn Powell, Alex Ray, Jonas Schneider, Szymon Sidor, Josh Tobin, Peter Welinder, Lilian Weng, and Wojciech Zaremba. Learning dexterous in-hand manipulation. *The International Journal of Robotics Research*, 39(1):3–20, 2020. doi: 10.1177/0278364919887447. URL <https://doi.org/10.1177/0278364919887447>.
- Kai Arulkumaran, Marc Peter Deisenroth, Miles Brundage, and Anil Anthony Bharath. Deep reinforcement learning: A brief survey. *IEEE Signal Process Mag.*, 34(6):26–38, 2017. doi: 10.1109/MSP.2017.2743240.
- Anton Bakhtin, Noam Brown, Emily Dinan, Gabriele Farina, Colin Flaherty, Daniel Fried, Andrew Goff, Jonathan Gray, Hengyuan Hu, Athul Paul Jacob, Mojtaba Komeili, Karthik Konath, Minae Kwon, Adam Lerer, Mike Lewis, Alexander H. Miller, Sasha Mitts, Adithya Renduchintala, Stephen Roller, Dirk Rowe, Weiyan Shi, Joe Spisak,

- Alexander Wei, David Wu, Hugh Zhang, and Markus Zijlstra. Human-level play in the game of `ijdiplomacyij` by combining language models with strategic reasoning. *Science*, 378(6624):1067–1074, 2022. doi: 10.1126/science.ade9097. URL <https://www.science.org/doi/abs/10.1126/science.ade9097>.
- Kshitij Bansal, Sarah Loos, Markus Rabe, Christian Szegedy, and Stewart Wilcox. HOList: An environment for machine learning of higher order logic theorem proving. In Kamalika Chaudhuri and Ruslan Salakhutdinov, editors, *Proceedings of the 36th International Conference on Machine Learning*, volume 97 of *Proceedings of Machine Learning Research*, pages 454–463, 2019. URL <https://proceedings.mlr.press/v97/bansal19a.html>.
- BigScience Workshop: T. Le Scao *et al.* BLOOM: A 176B-parameter open-access multilingual language model, 2023.
- Tom Brown, Benjamin Mann, Nick Ryder, Melanie Subbiah, Jared D Kaplan, Prafulla Dhariwal, Arvind Neelakantan, Pranav Shyam, Girish Sastry, Amanda Askell, Sandhini Agarwal, Ariel Herbert-Voss, Gretchen Krueger, Tom Henighan, Rewon Child, Aditya Ramesh, Daniel Ziegler, Jeffrey Wu, Clemens Winter, Chris Hesse, Mark Chen, Eric Sigler, Mateusz Litwin, Scott Gray, Benjamin Chess, Jack Clark, Christopher Berner, Sam McCandlish, Alec Radford, Ilya Sutskever, and Dario Amodei. Language models are few-shot learners. In H. Larochelle, M. Ranzato, R. Hadsell, M.F. Balcan, and H. Lin, editors, *Advances in Neural Information Processing Systems*, volume 33, pages 1877–1901. Curran Associates, Inc., 2020. URL https://proceedings.neurips.cc/paper_files/paper/2020/file/1457c0d6bfc4967418bfb8ac142f64a-Paper.pdf.
- Sébastien Bubeck, Varun Chandrasekaran, Ronen Eldan, Johannes Gehrke, Eric Horvitz, Ece Kamar, Peter Lee, Yin Tat Lee, Yuanzhi Li, Scott Lundberg, Harsha Nori, Hamid Palangi, Marco Tulio Ribeiro, and Yi Zhang. Sparks of artificial general intelligence: Early experiments with GPT-4, 2023. URL <https://arxiv.org/abs/2303.12712>.
- ChatGPT Example Chat. Share link of the chat record: <https://chat.openai.com/share/469a5885-3e37-404c-bd11-fca52b00a8eb>; see also Appendix B.
- Charles Q. Choi. 7 revealing ways AIs fail: Neural networks can be disastrously brittle, forgetful, and surprisingly bad at math. *IEEE Spectr.*, 58(10):42–47, 2021. doi: 10.1109/MSPEC.2021.9563958.
- Aakanksha Chowdhery, Sharan Narang, Jacob Devlin, Maarten Bosma, Gaurav Mishra, Adam Roberts, Paul Barham, Hyung Won Chung, Charles Sutton, Sebastian Gehrmann, Parker Schuh, Kensen Shi, Sasha Tsvyashchenko, Joshua Maynez, Abhishek Rao, Parker Barnes, Yi Tay, Noam Shazeer, Vinodkumar Prabhakaran, Emily Reif, Nan Du, Ben Hutchinson, Reiner Pope, James Bradbury, Jacob Austin, Michael Isard, Guy Gur-Ari, Pengcheng Yin, Toju Duke, Anselm Levskaya, Sanjay Ghemawat, Sunipa Dev, Henryk Michalewski, Xavier Garcia, Vedant Misra, Kevin Robinson, Liam Fedus, Denny Zhou, Daphne Ippolito, David Luan, Hyeontaek Lim, Barret Zoph, Alexander Spiridonov, Ryan Sepassi, David Dohan, Shivani Agrawal, Mark Omernick, Andrew M. Dai, Thanumalayan Sankaranarayanan Pillai, Marie Pellat, Aitor Lewkowycz, Erica Moreira,

- Rewon Child, Oleksandr Polozov, Katherine Lee, Zongwei Zhou, Xuezhi Wang, Brennan Saeta, Mark Diaz, Orhan Firat, Michele Catasta, Jason Wei, Kathy Meier-Hellstern, Douglas Eck, Jeff Dean, Slav Petrov, and Noah Fiedel. Palm: Scaling language modeling with pathways, 2022.
- Stéphane d’Ascoli, Pierre-Alexandre Kamienny, Guillaume Lample, and François Charton. Deep symbolic regression for recurrent sequences, 2022. URL <https://arxiv.org/abs/2201.04600>.
- Alex Davies, Petar Veličković, Lars Buesing, Sam Blackwell, Daniel Zheng, Nenad Tomašev, Richard Tanburn, Peter Battaglia, Charles Blundell, András Juhász, Marc Lackenby, Geordie Williamson, Demis Hassabis, and Pushmeet Kohli. Advancing mathematics by guiding human intuition with AI. *Nature*, 600(7887):70–74, 2021. doi: 10.1038/s41586-021-04086-x.
- Ernest Davis. The use of deep learning for symbolic integration: A review of (Lample and Charton, 2019), 2019. URL <https://arxiv.org/abs/1912.05752>.
- Iddo Drori, Sarah Zhang, Reece Shuttlesworth, Leonard Tang, Albert Lu, Elizabeth Ke, Kevin Liu, Linda Chen, Sunny Tran, Newman Cheng, Roman Wang, Nikhil Singh, Taylor L. Patti, Jayson Lynch, Avi Shporer, Nakul Verma, Eugene Wu, and Gilbert Strang. A neural network solves, explains, and generates university math problems by program synthesis and few-shot learning at human level. *Proc. Natl. Acad. Sci.*, 119(32):e2123433119, 2022. doi: 10.1073/pnas.2123433119.
- Alhussein Fawzi, Matej Balog, Aja Huang, Thomas Hubert, Bernardino Romera-Paredes, Mohammadamin Barekatalin, Alexander Novikov, Francisco J. R. Ruiz, Julian Schrittwieser, Grzegorz Swirszcz, David Silver, Demis Hassabis, and Pushmeet Kohli. Discovering faster matrix multiplication algorithms with reinforcement learning. *Nature*, 610(7930):47–53, 2022. doi: 10.1038/s41586-022-05172-4.
- Jiequn Han, Arnulf Jentzen, and Weinan E. Solving high-dimensional partial differential equations using deep learning. *Proc. Natl. Acad. Sci.*, 115(34):8505–8510, 2018. doi: 10.1073/pnas.1718942115.
- Hado van Hasselt, Arthur Guez, and David Silver. Deep reinforcement learning with double q-learning. In *Proceedings of the Thirtieth AAAI Conference on Artificial Intelligence*, AAAI’16, page 2094–2100, 2016.
- Yang-Hui He. Machine-learning mathematical structures. *International Journal of Data Science in the Mathematical Sciences*, 01(01):23–47, 2023. doi: 10.1142/S2810939222500010.
- Ziwei Ji, Nayeon Lee, Rita Frieske, Tiezheng Yu, Dan Su, Yan Xu, Etsuko Ishii, Ye Jin Bang, Andrea Madotto, and Pascale Fung. Survey of hallucination in natural language generation. *ACM Comput. Surv.*, 55(12), mar 2023. ISSN 0360-0300. doi: 10.1145/3571730. URL <https://doi.org/10.1145/3571730>.
- Cezary Kaliszyk, Josef Urban, Henryk Michalewski, and Mirek Olšák. Reinforcement learning of theorem proving. In *Proceedings of the 32nd International Conference on Neural Information Processing Systems*, NIPS’18, page 8836–8847, 2018.

- Guillaume Lample and François Charton. Deep learning for symbolic mathematics. In *International Conference on Learning Representations*, 2020. URL <https://openreview.net/forum?id=S1eZYeHFDS>.
- Joonho Lee, Jemin Hwangbo, Lorenz Wellhausen, Vladlen Koltun, and Marco Hutter. Learning quadrupedal locomotion over challenging terrain. *Science Robotics*, 5(47): eabc5986, 2020. doi: 10.1126/scirobotics.abc5986. URL <https://www.science.org/doi/abs/10.1126/scirobotics.abc5986>.
- Aitor Lewkowycz, Anders Andreassen, David Dohan, Ethan Dyer, Henryk Michalewski, Vinay Ramasesh, Ambrose Slone, Cem Anil, Imanol Schlag, Theo Gutman-Solo, Yuhuai Wu, Behnam Neyshabur, Guy Gur-Ari, and Vedant Misra. Solving quantitative reasoning problems with language models, 2022. URL <https://arxiv.org/abs/2206.14858>.
- Zuowen Liao and Shuijia Li. Solving nonlinear equations systems with an enhanced reinforcement learning based differential evolution. *Complex System Modeling and Simulation*, 2(1):78–95, 2022. doi: 10.23919/CSMS.2022.0003.
- F. Marquardt. Machine learning and quantum devices. *Lecture Notes for the 2019 Les Houches Summer School*, 2020.
- Joshua Maynez, Shashi Narayan, Bernd Bohnet, and Ryan McDonald. On faithfulness and factuality in abstractive summarization. In Dan Jurafsky, Joyce Chai, Natalie Schluter, and Joel Tetreault, editors, *Proceedings of the 58th Annual Meeting of the Association for Computational Linguistics*, pages 1906–1919, Online, July 2020. Association for Computational Linguistics. doi: 10.18653/v1/2020.acl-main.173. URL <https://aclanthology.org/2020.acl-main.173>.
- Aaron Meurer, Christopher P. Smith, Mateusz Paprocki, Ondřej Čertík, Sergey B. Kirpichev, Matthew Rocklin, AMiT Kumar, Sergiu Ivanov, Jason K. Moore, Sartaj Singh, Thilina Rathnayake, Sean Vig, Brian E. Granger, Richard P. Muller, Francesco Bonazzi, Harsh Gupta, Shivam Vats, Fredrik Johansson, Fabian Pedregosa, Matthew J. Curry, Andy R. Terrel, Štěpán Roučka, Ashutosh Saboo, Isuru Fernando, Sumith Kulal, Robert Cimrman, and Anthony Scopatz. Sympy: symbolic computing in Python. *PeerJ Comput. Sci.*, 3:e103, 2017. doi: 10.7717/peerj-cs.103.
- Volodymyr Mnih, Koray Kavukcuoglu, David Silver, Andrei A. Rusu, Joel Veness, Marc G. Bellemare, Alex Graves, Martin Riedmiller, Andreas K. Fidjeland, Georg Ostrovski, Stig Petersen, Charles Beattie, Amir Sadik, Ioannis Antonoglou, Helen King, Dharmashan Kumar, Daan Wierstra, Shane Legg, and Demis Hassabis. Human-level control through deep reinforcement learning. *Nature*, 518(7540):529–533, 2015. doi: 10.1038/nature14236.
- OpenAI. Gpt-4 technical report, 2023.
- OpenAI. ChatGPT 3.5. <https://chat.openai.com/>, 2024. Access: March 23, 2024.
- Stephen Ornes. Symbolic mathematics finally yields to neural networks. *Quanta Magazine*, 2020. URL <https://www.quantamagazine.org/symbolic-mathematics-finally-yields-to-neural-networks-20200520/>.

- Adam Paszke, Sam Gross, Francisco Massa, Adam Lerer, James Bradbury, Gregory Chanan, Trevor Killeen, Zeming Lin, Natalia Gimelshein, Luca Antiga, Alban Desmaison, Andreas Kopf, Edward Yang, Zachary DeVito, Martin Raison, Alykhan Tejani, Sasank Chilamkurthy, Benoit Steiner, Lu Fang, Junjie Bai, and Soumith Chintala. Pytorch: An imperative style, high-performance deep learning library. In H. Wallach, H. Larochelle, A. Beygelzimer, F. d'Alché-Buc, E. Fox, and R. Garnett, editors, *Advances in Neural Information Processing Systems*, volume 32, 2019. URL <https://proceedings.neurips.cc/paper/2019/file/bdbca288fee7f92f2bfa9f7012727740-Paper.pdf>.
- Julien Perolat, Bart De Vylder, Daniel Hennes, Eugene Tarassov, Florian Strub, Vincent de Boer, Paul Muller, Jerome T. Connor, Neil Burch, Thomas Anthony, Stephen McAleer, Romuald Elie, Sarah H. Cen, Zhe Wang, Audrunas Gruslys, Aleksandra Malysheva, Mina Khan, Sherjil Ozair, Finbarr Timbers, Toby Pohlen, Tom Eccles, Mark Rowland, Marc Lanctot, Jean-Baptiste Lespiau, Bilal Piot, Shayegan Omidshafiei, Edward Lockhart, Laurent Sifre, Nathalie Beauguerlange, Remi Munos, David Silver, Satinder Singh, Demis Hassabis, and Karl Tuyls. Mastering the game of stratego with model-free multiagent reinforcement learning. *Science*, 378(6623):990–996, 2022. doi: 10.1126/science.add4679. URL <https://www.science.org/doi/abs/10.1126/science.add4679>.
- Gabriel Poesia, WenXin Dong, and Noah Goodman. Contrastive reinforcement learning of symbolic reasoning domains. In A. Beygelzimer, Y. Dauphin, P. Liang, and J. Wortman Vaughan, editors, *Advances in Neural Information Processing Systems*, 2021. URL https://openreview.net/forum?id=ZarM_uLVyGw.
- David Silver, Julian Schrittwieser, Karen Simonyan, Ioannis Antonoglou, Aja Huang, Arthur Guez, Thomas Hubert, Lucas Baker, Matthew Lai, Adrian Bolton, Yutian Chen, Timothy Lillicrap, Fan Hui, Laurent Sifre, George van den Driessche, Thore Graepel, and Demis Hassabis. Mastering the game of go without human knowledge. *Nature*, 550(7676):354–359, 2017. ISSN 1476-4687. doi: 10.1038/nature24270. URL <https://doi.org/10.1038/nature24270>.
- David Silver, Thomas Hubert, Julian Schrittwieser, Ioannis Antonoglou, Matthew Lai, Arthur Guez, Marc Lanctot, Laurent Sifre, Dharshan Kumaran, Thore Graepel, Timothy Lillicrap, Karen Simonyan, and Demis Hassabis. A general reinforcement learning algorithm that masters chess, shogi, and go through self-play. *Science*, 362(6419):1140–1144, 2018. doi: 10.1126/science.aar6404. URL <https://www.science.org/doi/abs/10.1126/science.aar6404>.
- Richard S. Sutton and Andrew G. Barto. *Reinforcement Learning: An Introduction*. MIT Press, Cambridge, MA, second edition, 2018.
- Romal Thoppilan, Daniel De Freitas, Jamie Hall, Noam Shazeer, Apoorv Kulshreshtha, Heng-Tze Cheng, Alicia Jin, Taylor Bos, Leslie Baker, Yu Du, YaGuang Li, Hongrae Lee, Huaixiu Steven Zheng, Amin Ghafouri, Marcelo Menegali, Yanping Huang, Maxim Krikun, Dmitry Lepikhin, James Qin, Dehao Chen, Yuanzhong Xu, Zhifeng Chen, Adam Roberts, Maarten Bosma, Vincent Zhao, Yanqi Zhou, Chung-Ching Chang, Igor Krivokon, Will Rusch, Marc Pickett, Pranesh Srinivasan, Laichee Man, Kathleen Meier-Hellstern, Meredith Ringel Morris, Tulsee Doshi, Renelito Delos Santos, Toju Duke,

- Johnny Soraker, Ben Zevenbergen, Vinodkumar Prabhakaran, Mark Diaz, Ben Hutchinson, Kristen Olson, Alejandra Molina, Erin Hoffman-John, Josh Lee, Lora Aroyo, Ravi Rajakumar, Alena Butryna, Matthew Lamm, Viktoriya Kuzmina, Joe Fenton, Aaron Cohen, Rachel Bernstein, Ray Kurzweil, Blaise Aguera-Arcas, Claire Cui, Marian Croak, Ed Chi, and Quoc Le. Lamda: Language models for dialog applications, 2022.
- Hugo Touvron, Thibaut Lavril, Gautier Izacard, Xavier Martinet, Marie-Anne Lachaux, Timothée Lacroix, Baptiste Rozière, Naman Goyal, Eric Hambro, Faisal Azhar, Aurelien Rodriguez, Armand Joulin, Edouard Grave, and Guillaume Lample. Llama: Open and efficient foundation language models, 2023.
- Silviu-Marian Udrescu and Max Tegmark. AI Feynman: A physics-inspired method for symbolic regression. *Sci. Adv.*, 6(16), 2020. doi: 10.1126/sciadv.aay2631.
- Hado van Hasselt, Yotam Doron, Florian Strub, Matteo Hessel, Nicolas Sonnerat, and Joseph Modayil. Deep reinforcement learning and the deadly triad, 2018.
- Zhikang T. Wang and Masahito Ueda. Convergent and efficient deep Q learning algorithm. In *International Conference on Learning Representations*, 2022. URL <https://openreview.net/forum?id=0Jm3HZuj4r7>.
- Jason Wei, Xuezhi Wang, Dale Schuurmans, Maarten Bosma, brian ichter, Fei Xia, Ed H. Chi, Quoc V Le, and Denny Zhou. Chain of thought prompting elicits reasoning in large language models. In Alice H. Oh, Alekh Agarwal, Danielle Belgrave, and Kyunghyun Cho, editors, *Advances in Neural Information Processing Systems*, 2022. URL https://openreview.net/forum?id=_VjQlMeSB_J.
- Stephen Wolfram. ChatGPT gets its “Wolfram superpowers”! Stephen Wolfram Writings, 2023a. URL <https://writings.stephenwolfram.com/2023/03/chatgpt-gets-its-wolfram-superpowers/>.
- Stephen Wolfram. Wolfram|Alpha as the way to bring computational knowledge superpowers to ChatGPT. Stephen Wolfram Writings, 2023b. URL <https://writings.stephenwolfram.com/2023/01/wolframalpha-as-the-way-to-bring-computational-knowledge-superpowers-to-chatgpt/>.
- Peter R. Wurman, Samuel Barrett, Kenta Kawamoto, James MacGlashan, Kaushik Subramanian, Thomas J. Walsh, Roberto Capobianco, Alisa Devlic, Franziska Eckert, Florian Fuchs, Leilani Gilpin, Piyush Khandelwal, Varun Kompella, HaoChih Lin, Patrick MacAlpine, Declan Oller, Takuma Seno, Craig Sherstan, Michael D. Thomure, Houmehr Aghabozorgi, Leon Barrett, Rory Douglas, Dion Whitehead, Peter Dürr, Peter Stone, Michael Spranger, and Hiroaki Kitano. Outracing champion gran turismo drivers with deep reinforcement learning. *Nature*, 602(7896):223–228, 2022. ISSN 1476-4687. doi: 10.1038/s41586-021-04357-7. URL <https://doi.org/10.1038/s41586-021-04357-7>.
- Run-Fa Zhang and Sudaog Bilige. Bilinear neural network method to obtain the exact analytical solutions of nonlinear partial differential equations and its application to p-gbpk equation. *Nonlinear Dynamics*, 95(4):3041–3048, 2019. ISSN 1573-269X. doi: 10.1007/s11071-018-04739-z. URL <https://doi.org/10.1007/s11071-018-04739-z>.

Run-Fa Zhang and Ming-Chu Li. Bilinear residual network method for solving the exactly explicit solutions of nonlinear evolution equations. *Nonlinear Dynamics*, 108(1):521–531, 2022. ISSN 1573-269X. doi: 10.1007/s11071-022-07207-x. URL <https://doi.org/10.1007/s11071-022-07207-x>.

Run-Fa Zhang, Ming-Chu Li, Jian-Yuan Gan, Qing Li, and Zhong-Zhou Lan. Novel trial functions and rogue waves of generalized breaking soliton equation via bilinear neural network method. *Chaos, Solitons & Fractals*, 154:111692, 2022. ISSN 0960-0779. doi: <https://doi.org/10.1016/j.chaos.2021.111692>. URL <https://www.sciencedirect.com/science/article/pii/S0960077921010468>.